Ferdows *et al.*
Journal of Engineering and Applied Science (2024) 71:57
https://doi.org/10.1186/s44147-024-00388-9

Journal of Engineering and Applied Science

RESEARCH Open Access

Three-dimensional boundary layer flow and heat/mass transfer through stagnation point flow of hybrid nanofluid

Mohammad Ferdows[1*], MD. Shamshuddin[2], Ahmed Mohammed Rashad[3], Md Gulum Murtaza[4] and Sulyman Olakunle Salawu[5]

*Correspondence:
ferdows@du.ac.bd

[1] Research Group of Fluid Flow Modeling and Simulation, Department of Applied Mathematics, University of Dhaka, Dhaka 1000, Bangladesh
[2] Department of Computer Science and Artificial Intelligence (Mathematics), SR University, Warangal, Telangana State 506371, India
[3] Department of Mathematics, Faculty of Science, Aswan University, Aswan 81528, Egypt
[4] Department of Mathematics, Comilla University, Cumilla 3506, Bangladesh
[5] Department of Mathematics, Bowen University, Iwo, Nigeria

Abstract

This project covers the investigation of the boundary layer flow of a hybrid nanofluid past a biaxial stretching/shrinking sheet. The hybrid nanofluid consists of copper (Cu) and alumina (Al_2O_3) nanoparticles, which are diluted into water to form $Cu - Al_2O_3 -$ water hybrid nanofluid. The governing partial differential equations (PDEs) are derived from Navier-Stokes equations. The system of PDEs is reduced to a system of ordinary differential equations using an appropriate similarity transformation. MATLAB's bvp4c function is used to numerically solve the resulting system of governing ordinary differential equations. The aim of this study is to gain a comprehensive understanding of the intricate behavior displayed by hybrid nanofluids on the stagnant directed flow of extended/shrunk flat surfaces, considering the effects of Brownian motion, thermophoresis, and various nanoparticles. The generated numerical results of flow profiles, skin friction coefficient, and Nusselt number have been presented graphically and discussed in the relevance of the governing parameters contributing to the flow. The outcomes reveal that the velocity components are reduced with increasing Al_2O_3- water nanofluid volume fraction. A monotonical increase in the parameters stretching/shrinking and suction/injection with a corresponding rise in both nanoparticles volume fraction propels heat gradient rate. An increase in the Schmidt numbers encourages a mass transfer field due to an enhanced boundary viscosity. The validation of numerical results is done with previously published results. Through our results, we have found that the performance of a hybrid nanofluid is more significant than other fluids. In addition, this study enhances the progress of theoretical comprehension by endeavoring to resolve the intricate interplay between fluid dynamics and thermal characteristics through the utilization of numerical approaches.

Keywords: Boundary layer flow, Stagnation point flow, Hybrid nanofluid, Nanoparticles

Introduction

Heat transfer improvement research has gotten much attention for the past few years. Thermal researchers have proposed that nano-sized metallic or nonmetallic particles be added to the base fluid to increase thermal conductivity since nanoparticles have a better

thermal conductivity than the base fluid. Nanofluid is the name given to the resultant combination that has improved physical and chemical characteristics. Choi [1] studied the phenomena of nano-particles floating in a base fluid and coined the term "nanofluid". The most crucial aspect of nanofluid is that coagulation may be reduced. The use of suitable surfactants and homogeneous particle dispersion can further reduce congestion. The transport mechanism of nanofluids greatly improves the thermal performance of various base liquids. The inclusion of certain base materials induces the breakdown of metallic particles in nanofluids. The metallic particles are capable of trapping particles that are small in size and diameter. The main purpose of nanoparticles is to enhance the heat transfer phenomena. They have various applications in the industrial framework and applied thermal engineering. Possible uses of nanofluids include cooling systems, hydraulic systems, solar panels, power generation, etc. Several researchers have recently studied the synthesis, production, and characterization of various nanofluids for diverse heat transfer applications. Many numerical and experimental findings have been presented on different amalgamations of nanoparticles and base fluids. Al, Cu, Fe (metals), Al_2O_3, CuO (metal oxides), SiO_2, and TiO_2 (nanoparticles) are some of the most often utilized nanoparticles (semiconductors). Many references to nanofluids may be found in literature, which is worth noting [2–4].

A hybrid nanofluid is a homogenous combination of duplet or supplementary nanoparticles with unique physical and chemical relations. As a result of the combined impact, the fundamental goal of hybrid nanofluids is to produce results in thermophysical, hydrodynamic, and heat transmission characteristics as contrasted to mono nanofluids [5]. Even at low particle densities, the requisite heat transfer effect may be achieved by hybridizing the suitable mix of nanoparticles [6]. Because hybrid nanofluids are a new fluid type, more reviews must be done on their synthesis and processing [7]. Review publications such as [8–10] provide a complete overview of hybrid nanofluids for additional study. The numerical analyses on the hybrid nanofluid are regarded as a novel addition to the boundary layer flow theory by the researchers. For further information, consult [8–10], which provide a complete overview of hybrid nanofluids. The numerical investigations on the hybrid nanofluid have been regarded as a significant contribution to the boundary layer flow theory by the researchers. Devi and Devi [11], for example, investigated the flow of a hybrid nanofluid through a stretched surface using $Cu–Al_2O_3$ nanoparticles with magnetic effects. They discovered that the heat transfer rate of a hybrid nanofluid is higher than that of a conventional nanofluid. The problem was then expanded to a three-dimensional flow subject to the Newtonian heating condition [12]. Rostami et al. [13] investigated a silica–alumina hybrid nanofluid's mixed convective flow at a stagnation point. Waini et al. [14] studied the dual approaches to the flow of a hybrid nanofluid with heat exchange along an extending or contracting surface while acknowledging unsteady flow.

Extrusion operations, expanding balloons, an extension of pseudopods, glass blowing, hot rolling, wire drawing, paper manufacturing, glass blowing, plastic film drawing, and glass-fiber production are all examples of sectors where flow due to a stretched surface is a significant issue. The heat transmission rate at the stretching surface determines the final product's quality. Wang [15] was the first to investigate three-dimensional flow across a biaxially stretched flat surface using an axisymmetric stretching surface. Using

the similarity transformation, the Navier-Stokes equations are reduced to a set of nonlinear ordinary differential equations, which are then numerically integrated using the shooting technique. After that, [16] expanded this study to include unsteady flow and heat and species transmission. In addition, other writers, such as [17–20], have studied flow across a biaxial flat surface. However, the previous sources should have considered the fluid's lateral movements away from the surface. It's worth noting that [21] examined uniform flow across a biaxial stretching surface with the fluid moving laterally away from the surface. According to the author, the lateral stretching enhanced the net shear stress and drag caused by the uniform flow. Using the nanofluid model given by [22, 23] expanded this study to nanofluid flow across a stretching/shrinking sheet. Abbas et al. [24] predicted the significance of MHD and slip effects with the interaction of hybrid nanoparticles in stagnated points. Nadeem et al. [25] visualized the nanomaterial properties with base viscoelastic micropolar fluid in an extended sheet. Abbas et al. [26] disclosed the hybrid nanofluid thermal prediction in nonlinear curved surfaces via numerical analysis. Li et al. [27] determined the hybrid nanomaterials base maxwell micropolar analysis with heat transfer phenomenon. Abbas and Shatanawi [28] included the Micropolar-Casson analysis numerically over exponentially extending Riga plate with the support of nanofluid.

Therefore, the aim of the present article is to investigate the uniform flow and heat transmission of a hybrid nanofluid over a permeable biaxial stretching/shrinking sheet using copper (Cu) and alumina (Al_2O_3) nanoparticles. To create a hybrid nanofluid, these nanoparticles are suspended in water. The study of these fluid models has gained significant importance in the present techno-industrial period due to their increasing demand in various technical and manufacturing processes. The flux mixture can be mathematically described by a complex equation that requires a numerical solution. To solve this equation, the transformation governing equations along with the corresponding boundary conditions are solved numerically using the boundary value problem solver (bvp4c) in MATLAB function. The current numerical findings are compared to previously released data for validation reasons. The findings may be highly beneficial in raising the energy efficiency of thermal systems.

Methods

Geometry formulation

Figure 1 depicts the constant flow of a hybrid nanofluid across a permeable transverse direction flexion and extension flat surface, with x- and y-coordinates in the surface plane and z measured in the plane perpendicular to the x-y plane. The flat surface is stretched/shrunk continuously in both the x- and y-directions with the velocities $u = u_w(x, t)$ and $v = v_w(x, t)$. Far from the surface at $z \to \infty$, there is a uniform flow of velocity $u_e = U$. Another assumption is that the constant mass flux velocity is $w = w_0$, where $w_0 < 0$ is for suction and $w_0 > 0$ is for injection. Because nanofluids are manufactured as a stable combination of nanoparticles and the base fluid, the size of the particles in hybrid nanofluids is presumed to be uniform, and the effects of nanoparticle aggregation on thermophysical characteristics are neglected.

Under these conditions, the governing equations of the hybrid nanofluid are [12, 21, 23]:

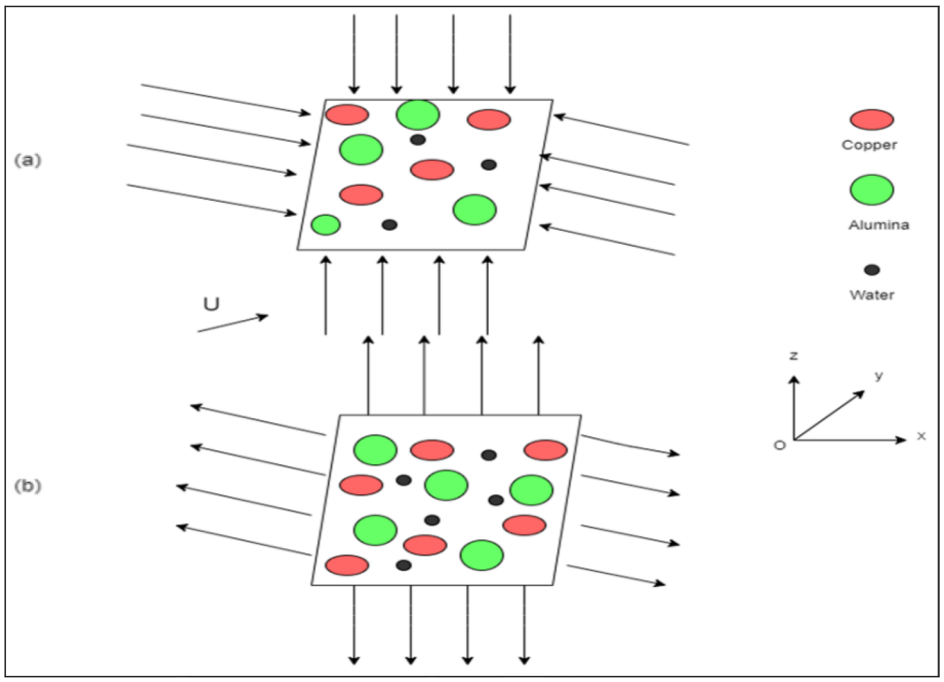

Fig. 1 A tangible representation and coordinate system. **a** Shrinking sheet. **b** Stretching sheet

$$\frac{\partial u}{\partial x}+\frac{\partial v}{\partial y}+\frac{\partial w}{\partial z}=0 \tag{1}$$

$$\frac{\partial u}{\partial t}+u\frac{\partial u}{\partial x}+v\frac{\partial u}{\partial y}+w\frac{\partial u}{\partial z}=-\frac{1}{\rho_{hnf}}\frac{\partial p}{\partial x}+\frac{\mu_{hnf}}{\rho_{hnf}}\nabla^2 u \tag{2}$$

$$\frac{\partial v}{\partial t}+u\frac{\partial v}{\partial x}+v\frac{\partial v}{\partial y}+w\frac{\partial v}{\partial z}=-\frac{1}{\rho_{hnf}}\frac{\partial p}{\partial y}+\frac{\mu_{hnf}}{\rho_{hnf}}\nabla^2 v \tag{3}$$

$$\frac{\partial w}{\partial t}+u\frac{\partial w}{\partial x}+v\frac{\partial w}{\partial y}+w\frac{\partial w}{\partial z}=-\frac{1}{\rho_{hnf}}\frac{\partial p}{\partial z}+\frac{\mu_{hnf}}{\rho_{hnf}}\nabla^2 w \tag{4}$$

$$\frac{\partial T}{\partial t}+u\frac{\partial T}{\partial x}+v\frac{\partial T}{\partial y}+w\frac{\partial T}{\partial z}=\propto_{hnf}\nabla^2 T+\frac{(\boldsymbol{\rho c_p})_{\boldsymbol{hnf}}}{(\boldsymbol{\rho c_p})_{\boldsymbol{f}}}\left\{\begin{array}{c}\boldsymbol{D_B}\left(\frac{\partial C}{\partial x}\frac{\partial T}{\partial x}+\frac{\partial C}{\partial y}\frac{\partial T}{\partial y}+\frac{\partial C}{\partial z}\frac{\partial T}{\partial z}\right)+\\ \frac{\boldsymbol{D_T}}{\boldsymbol{T_\infty}}\left[\left(\frac{\partial T}{\partial x}\right)^2+\left(\frac{\partial T}{\partial y}\right)^2+\left(\frac{\partial T}{\partial z}\right)^2\right]\end{array}\right\} \tag{5}$$

$$\frac{\partial C}{\partial t}+u\frac{\partial C}{\partial x}+v\frac{\partial C}{\partial y}+w\frac{\partial C}{\partial z}=\boldsymbol{D_B}\nabla^2 C+\frac{\boldsymbol{D_T}}{\boldsymbol{T_\infty}}\nabla^2 T \tag{6}$$

Initial and Boundary conditions are the following:

$$\left.\begin{array}{c} t<0:\mathrm{u}(\mathrm{x},\mathrm{y},\mathrm{t})=0,\mathrm{v}(\mathrm{x},\mathrm{y},\mathrm{t})=0,\mathrm{w}(\mathrm{x},\mathrm{y},\mathrm{t})=0,T=T_\infty,C=\boldsymbol{C}_\infty \text{ for any x,y,z} \\ t\geq 0:u=u_w(x,t)=a\lambda x,v=v_w(y,t)=a\lambda x,w=w_w=w_0,T=T_W, \\ D_B\frac{\partial C}{\partial z}+\frac{D_T}{T_\infty}\frac{\partial T}{\partial z}\,at\,z=0 \\ u=u_e\to U,v=v_e\to 0,w=w_e\to 0,T\to \boldsymbol{T}_\infty,C\to \boldsymbol{C}_\infty asz\to\infty \end{array}\right\} \tag{7}$$

Mathematical analysis and similarity transformation

Use the following similarity variables [21, 23]:

$$the\,the\ \left.\begin{array}{c} u=axf'(\eta)+\mathrm{U}\,\mathrm{h}(\eta),v=ayf'(\eta),w=-2\sqrt{a\upsilon_f}f(\eta) \\ \theta(\eta)=\frac{T-T_\infty}{T_w-T_\infty},\phi(\eta)=\frac{C-C_\infty}{C_w-C_\infty},\eta=\sqrt{a/\upsilon_f} \end{array}\right\} \tag{8}$$

Using the above, we get

$$\frac{c_1}{c_2}f'''+2ff'-f'^2=0 \tag{9}$$

$$\frac{c_1}{c_2}h''+2fh'-hf'=0 \tag{10}$$

$$c_3c_4\frac{1}{Pr}\theta''+2f\theta'+c_3Nb\phi'\theta'+c_3Nt\theta'^2=0 \tag{11}$$

$$\phi''+2Scf\phi'+\frac{Nb}{Nt}\theta''=0 \tag{12}$$

Boundary conditions:

$$\left.\begin{array}{c} f(0)=S,f'(0)=\lambda,h(0)=0,\theta(0)=1,Nb\phi'(0)+Nt\theta'(0)=0 \\ f'(\eta)\to 0,h(\eta)\to 1,\theta(\eta)\to 0,\phi(\eta)\to 0\,as\,\eta\to\infty \end{array}\right\} \tag{13}$$

Where

$$\left.\begin{array}{c} Pr=\frac{\upsilon_f(\rho C_p)_f}{k_f},Nb=\frac{\tau D_B(C_w-C_\infty)}{\upsilon_f},Nt=\frac{\tau D_T(T_w-T_\infty)}{T_\infty\upsilon_f},S=-\frac{w_0}{2\sqrt{a\upsilon_f}}, \\ Sc=\frac{\upsilon_f}{D_B},\tau=\frac{(\rho Cp)_s}{(\rho Cp)_f} \end{array}\right\} \tag{14}$$

Equation (14) represents the dimensionless terms obtained from Eqs. (9)–(13) are named (Pr) Prandtl number, Brownian motion parameter (Nb), thermophoresis parameter (Nt), surface mass parameter (S) with suction ($S>0$) and injection ($S<0$), Schmidt number (Sc), and ratio of nanoparticle materials to effective heat capacity (τ).

The nanofluid constants are defined as follows:

$$\left.\begin{array}{c} c_1=\frac{\mu_{hnf}}{\mu_f},c_2=\frac{\rho_{hnf}}{\rho_f},c_3=\frac{(\rho Cp)_f}{(\rho Cp)_{hnf}},c_4=\frac{k_{hnf}}{k_f} \end{array}\right\} \tag{15}$$

Physical interests like Skin friction coefficient, Nusselt number, and Sherwood number in dimensionless form are defined as:

$$\left.\begin{aligned} Re_x^{\frac{1}{2}} C_{fx} &= \frac{\mu_{hnf}}{\mu_f}\left[f''(0) + \frac{U}{ax}h'(0)\right], \\ Re_x^{-\frac{1}{2}} Nu_x &= -\frac{k_{hnf}}{k_f}\theta'(0), \\ Re_x^{-\frac{1}{2}} Sh_x &= -\phi'(0) \end{aligned}\right\} \tag{16}$$

Where subscript base, cap $R\ e$, end base, sub x equals numerator, cap U sub w, x end numerator, over upsilon sub f is the local Reynolds number and the thermophysical characteristics of the base fluid, and nanoparticles and characteristics of nanofluid are presented in Tables 1 and 2.

Solution procedure

The boundary conditions (13) and the resultant nonlinear ordinary differential Eqs. (9)–(12) are calculated using the bvp4c solver in the MATLAB program. For this method, first transformed the higher-order system of equations is transformed into the first-order system of equations. Further calculations in Bvp4c set the guess value of all known and unknown functions. Starting with a guess at an initial mesh point, the results are generated by increasing the step size until the requisite precision is reached. Based on the values of the parameters used, the appropriate beginning estimate and boundary layer thickness must be chosen. The proposed numerical code is known as the following:

$$f = y(1) \tag{17}$$

$$f' = y(2) \tag{18}$$

$$f'' = y(3) \tag{19}$$

$$f''' = \frac{c_2}{c_1}(-2y(1)y(2) + (y(2))^2 \tag{20}$$

$$h = y(4) \tag{21}$$

Table 1 Thermophysical characteristics of water and nanoparticles [7, 11, 12]

Thermophysical characteristics	Base fluid	Nanoparticles	
	Water	*Cu*	Al_2O_3
$\rho(kg/m\hat{}3)$	997.1	8933	3970
C_p(J/kgK)	4179	385	765
k(W/m K)	0.613	400	40
$\beta \times 10^{-5}$(1/K)	21	1.67	0.85
Prandtl number	6.2		

Table 2 Characteristics of nanofluid hybrid nanofluid [11, 12]

Properties	Nanofluid	Hybrid nanofluid
Density	$\rho_{nf} = (1-\varphi_1)\rho_f + \varphi_1\rho_{n1}$	$\rho_{hnf} = (1-\varphi_2)[(1-\varphi_1)\rho_f + \varphi_1\rho_{n1}] + \varphi_2\rho_{n2}$
Dynamic viscosity	$\mu_{nf} = \frac{\mu_f}{(1-\varphi_1)^{2.5}}$	$\mu_{hnf} = \frac{\mu_f}{(1-\varphi_1)^{2.5}(1-\varphi_2)^{2.5}}$
Heat capacity	$(\rho C_p)_{nf} = (1-\varphi_1)(\rho C_p)_f + \varphi_1(\rho C_p)_{n1}$	$(\rho C_p)_{hnf} = (1-\varphi_2)\left[(1-\varphi_1)(\rho C_p)_f + \varphi_1(\rho C_p)_{n1}\right] + \varphi_2(\rho C_p)_{n2}$
Thermal conductivity	$\frac{k_{nf}}{k_f} = \frac{k_{n1}+2k_f-2\varphi_1(k_f-k_{n1})}{k_{n1}+2k_f+\varphi_1(k_f-k_{n1})}$	$\frac{k_{hnf}}{k_{nf}} = \frac{k_{n2}+2k_{nf}-2\varphi_2(k_{nf}-k_{n2})}{k_{n2}+2k_{nf}+\varphi_2(k_{nf}-k_{n2})}$

$$h' = y(5) \tag{22}$$

$$h'' = \frac{c_2}{c_1}\left(-2y(1)y(5) + y(4)y(2)\right) \tag{23}$$

$$\theta' = y(7) \tag{24}$$

$$\theta'' = \frac{Pr}{c_4}\left(\left(-\frac{2y(1)y(7)}{c_3}\right) - Nby(9)y(7) - Nt\left(y(7)\right)^2\right) \tag{25}$$

$$\phi' = y(9) \tag{26}$$

$$\phi'' = -2Scy(9)y(1) - \frac{Nb}{Nt}\frac{Pr}{c_4}\left(\left(-\frac{2y(1)y(7)}{c_3}\right) - Nby(9)y(7) - Nt\left(y(7)\right)^2\right) \tag{27}$$

Boundary conditions:

$$\left.\begin{array}{c} y_a(1) - S, y_a(2) - \lambda, y_a(4), y_a(6) - 1, Nby_a(9) + +Nty_a(7), \\ y_b(2), y_b(4) - 1, y_b(6), y_b(8) \end{array}\right\} \tag{28}$$

Previous research has successfully calculated and confirmed the use of bvp4c codes to solve both steady flow and normalizing stability equations. The computations in this study are done using$\eta_\infty = 5$. Tolerance is considered in this problem 10^{-4}. As is generally the case in boundary layer analysis, the progressive boundary conditions go to infinity and are substituted with those at a large but finite value has no significant change in velocity, temperature, etc., occurs (Fig. 2).

Numerical validation

In order to estimate the validity of the numerical analysis, a comparison of skin friction $-f''(0)$ and $h'(0)$ as well as the heat transfer coefficient in Table 3. The findings for $f''(0), h'(0)$ and $-\theta'(0)$ were compared to those previously published results [21] for $\varphi_1 = \varphi_2 = 0,\ Pr = 7, Nb = 0.5, Nt = 0.3, \lambda = 1, Sc = 1, S = 2$ to ensure the validity and correctness of the current study. This table shows that the above-mentioned paper and this table are in good accord.

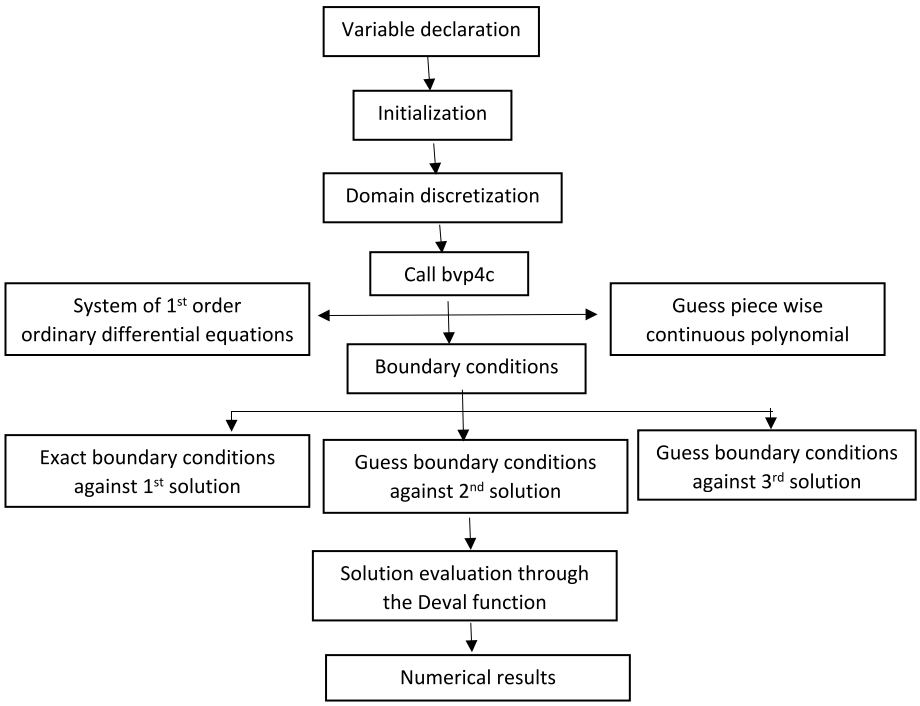

Fig. 2 Flow chart of the bvp4c procedure

Table 3 Comparison of $-f''(0), h'(0)$ *and* $\theta'(0)$ with Wang [21] for various values S with specific values of $\varphi_1 = \varphi_2 = 0, Pr = 7, Nb = 0.5, Nt = 0.3, \lambda = 1, Sc = 1, S = 2$

	$f''(0)$	$h\prime(0)$	$-\theta\prime(0)$
Present	−1.1737	0.6654	2.6008
Wang [21]	−1.1737	0.6653	2.7230

Results and discussion

In this article, the heat and mass transfer analysis find out $Cu - Al_2O_3-$ water hybrid nanofluid in stagnation point flow of biaxial stretching/shrinking sheet geometry. Aqueous-based fluid medium considers two kinds of nanoparticles (cap C u minus subscript base, cap A. l, end base, sub 2, cap O sub 3). Further two-phase model is incorporated in the study. The reduced nonlinear Eqs. (9)–(12), along with boundary conditions Eq. (13) are numerically solved with MATLAB's bvp4c function to generate results. The physical, vital quantities flow profiles such as Skin friction $f''(0)$, Nusselt number $\theta'(0)$, Shearwood number $\phi'(\eta)$, velocity $f'(\eta)$ and $h(\eta)$, temperature $\theta(\eta)$ and volume fraction $\phi(\eta)$ profiles are investigated, for different values of the parameters and depicted through graphs.

The response of the flow dimensions for the $Al_2O_3 - Cu/$ water hybrid nanofluid to varying nanoparticle volume fraction is demonstrated in Figs. 3, 4, and 5. A decrease in the flow momentum $f'(\eta)$ and axial flow momentum $h(\eta)$ are obtained due to a rising

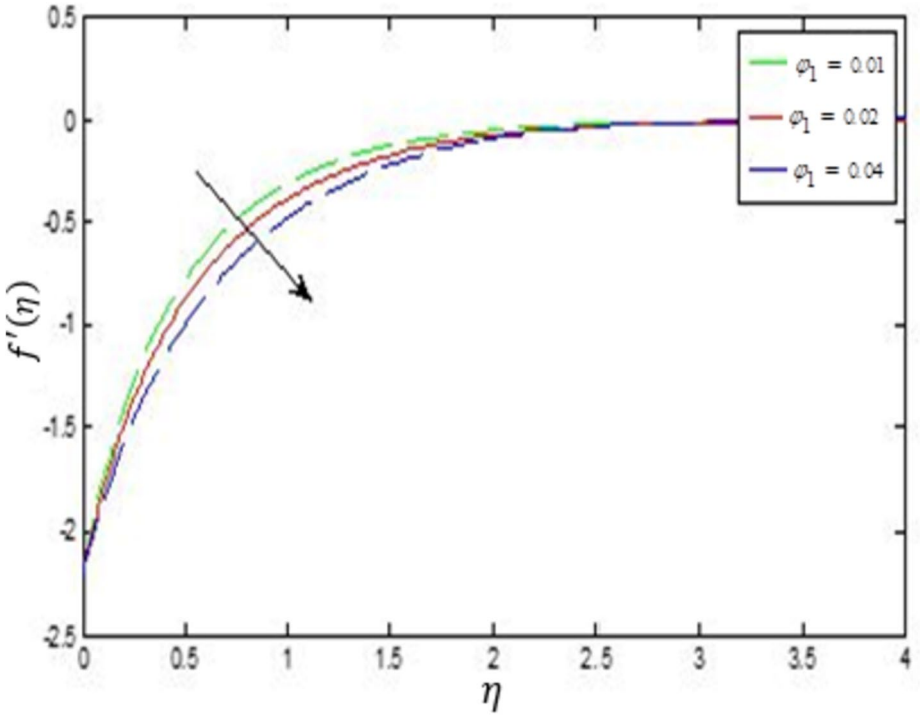

Fig. 3 The velocity aspects $f'(\eta)$ for different values of φ_1

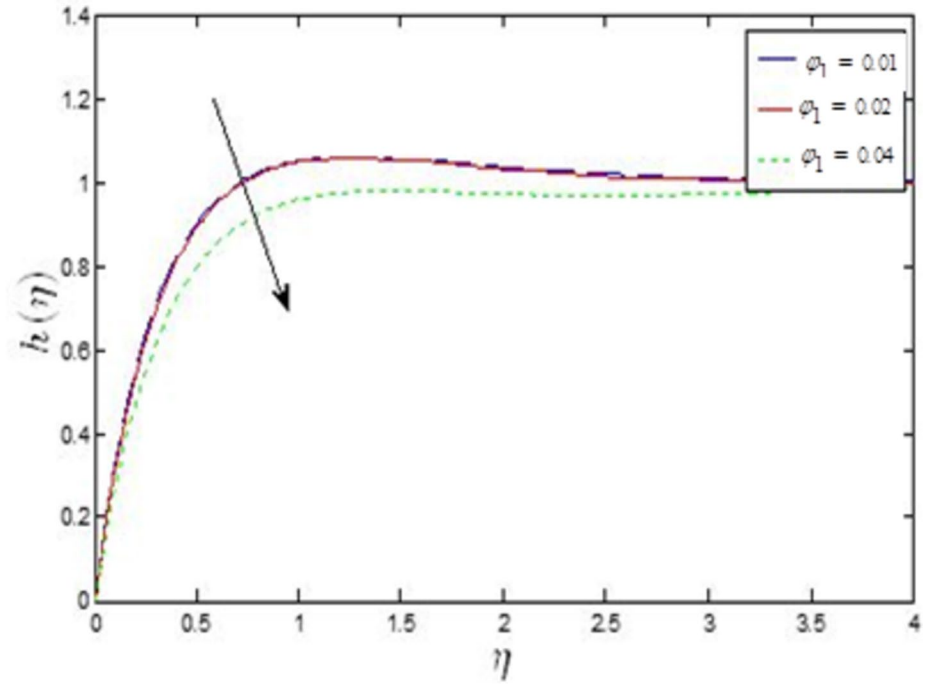

Fig. 4 The velocity aspects $h(\eta)$ for different values of φ_1

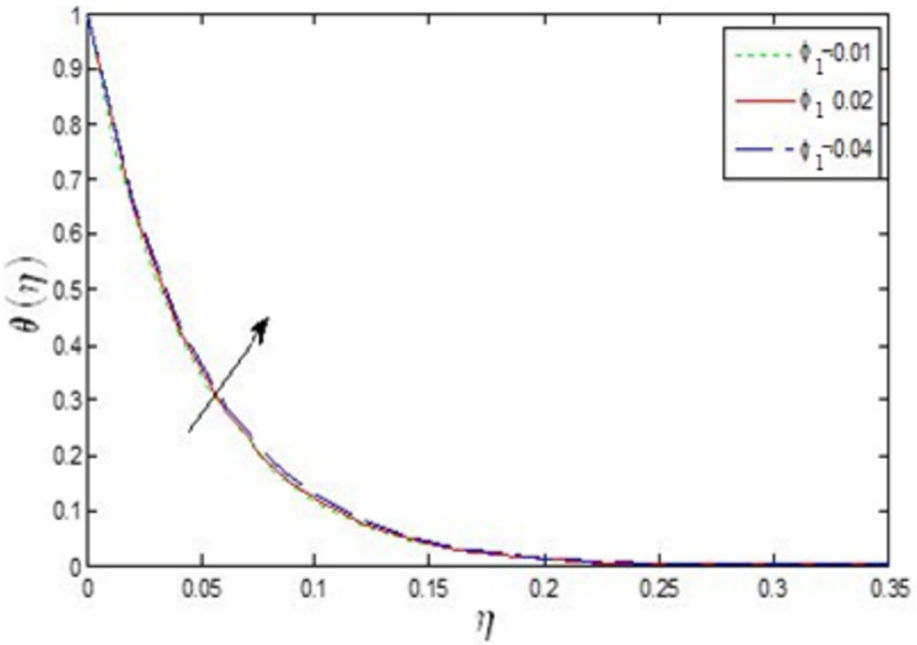

Fig. 5 The temperature aspects $\theta(\eta)$ for various values of φ_1

stretchy sheet that caused the ambient heat diffusion as seen in Figs. 3 and 4. As such, nanoparticle interaction is damped as a result of an enhanced molecular bonding and the fluid flow stagnation point. This resulted in a boosted fluid bonding force, and heat dissipation discouraged the flow velocity along the boundless stream domain, thereby decreasing the velocity profiles. Meanwhile, in Fig. 5, the temperature distribution is propelled with a rising nanoparticle volume fraction, the effect is less pronounced due to the combined influence of the stagnation point and wall stretching velocity that dominated the heat generation. Hence, the temperature profile is gradually enhanced. The respective impact of the Brownian motion (Nb) and the thermophoresis term (Nt) on the heat distribution and species reaction are depicted in Figs. 6, 7, 8, and 9. Both the heat and mass distributions decreased with an increasing Brownian motion value as noticed in Figs. 6 and 7. The random collision of nanoparticles with the fluid surrounding molecules is reduced across the flow regime. The suspended nanoparticles in water-based fluid are restricted in movement due to lower heat generation and fluid stagnation. Whereas the temperature profile and mass transfer field are raised as the thermophoresis values are boosted as offered in Figs. 8 and 9. The thermophoresis effect is experienced in moving particle mixture, in which particles respond differently to heat gradient force. This phenomenon moves light and heavy particles to hot and cold regions correspondingly. The force generated caused the $Al_2O_3/Cu-$ water hybrid nanofluid heat distribution and species mixtures field to increase momentously all over the stream regime as observed in the plots.

Figure 10 presents the impact of a rise in the Schmidt number on the mass transfer. The species concentration distribution is enhanced due to a rising viscosity of the mass boundary layer. As seen, the kinematic viscosity ratio to the molecular diffusion coefficient is inspired to raise the concentration profile. The hybrid nanofluids

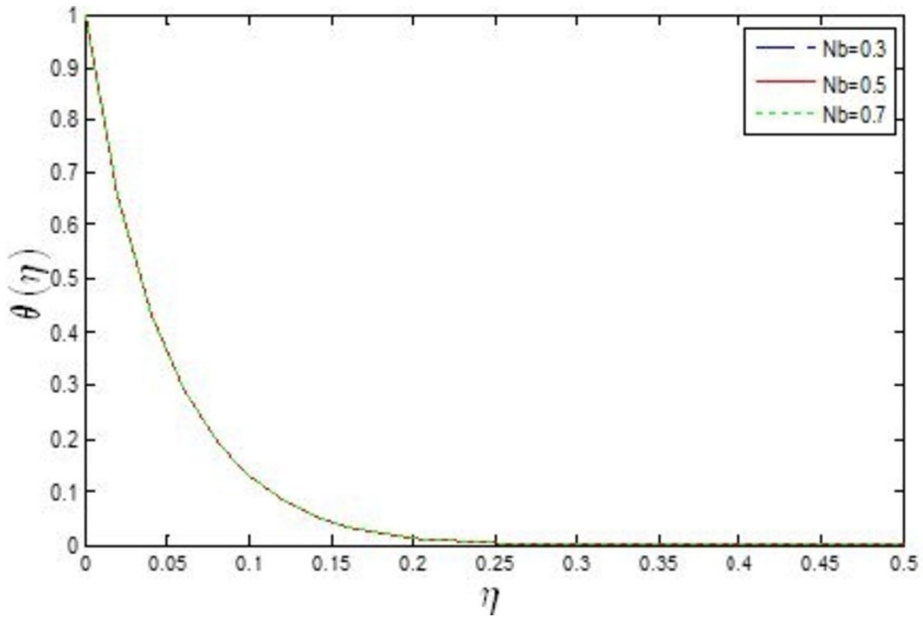

Fig. 6 Discrepancy of $\theta(\eta)$ for different values of *Nb*

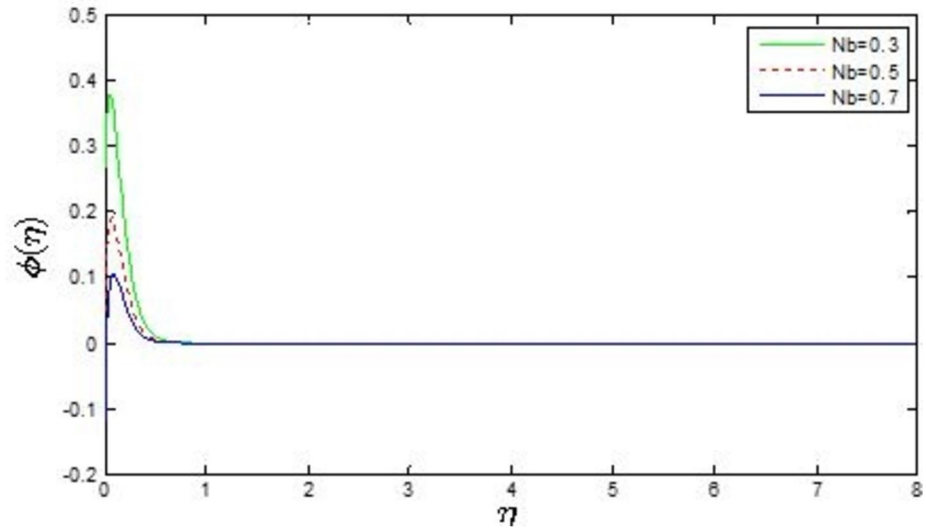

Fig. 7 Discrepancy of $\phi(\eta)$ for different values of *Nb*

chemical mixtures are encouraged to stimulate heat transfer, thereby raising the mass transfer. In Figs. 11, 12, and 13, the influence of Al_2O_3(alumina) nanoparticle fractional volume on the engineering wall quantities is established. The wall effect along an increasing stretchy sheet for different numbers of φ_1 discouraged the wall friction, the nanoparticles exert force on the water base fluid. Thus, the momentum boundary viscosity is enhanced, decreasing the wall friction. However, the term φ_1 increased the temperature gradient due to rapid changes in the temperature around a nanoparticle position. This leads to an upsurge in the Nusselt number along the increasing pliable sheet. Meanwhile, the mass gradient profile in Fig. 13 reduced for

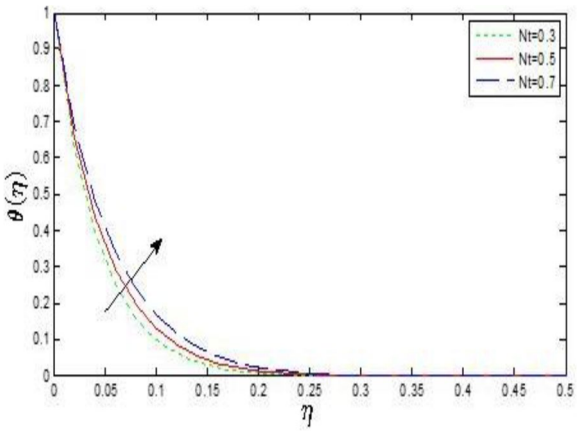

Fig. 8 Discrepancy of $\theta(\eta)$ for different values of *Nt*

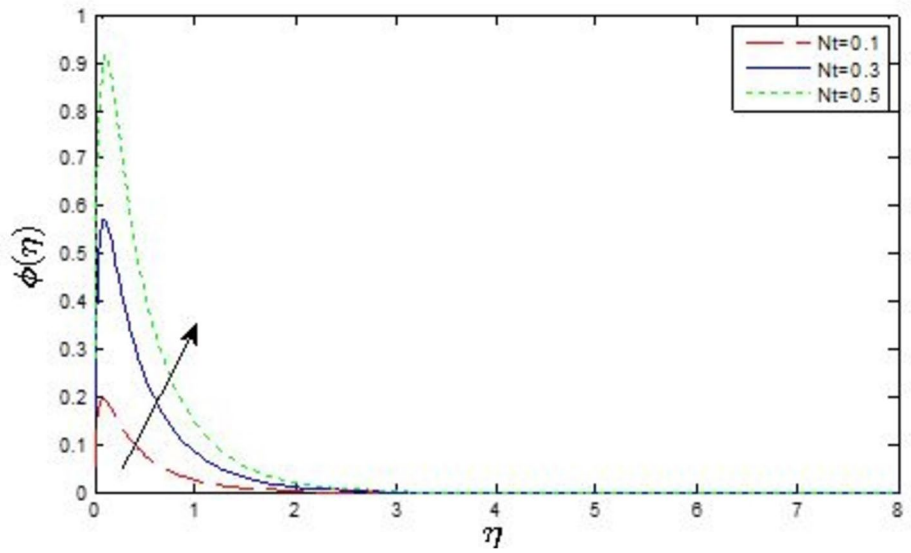

Fig. 9 Discrepancy of $\phi(\eta)$ for different values of *Nt*

a rising value of φ_1 along the far stream of, cap A. l, end base, sub 2, cap O sub 3nanoparticle difference creates chemical molecular mixtures, stimulating particles bodding, thereby reducing the Sherwood number field.

Likewise, Figs. 14, 15, and 16 show the strength of the *Cu* (copper) volume fraction variation across the raised stretching wall for the plate friction, thermal gradient, and Sherwood number. The effect of φ_2 on the physical quantities is more pronounced for Cu nanoparticles than the Al_2O_3 nanoparticles volume fraction φ_1 for the respective physical engineering quantities. This is because the dispersion of Cu nanoparticles in water caused particle collision and heat generation than the subscript base, heat generation than the Al_2O_3 nanoparticle. From Figs. 17, 18, 19, 20, 21, and 22, the respective effect of Al_2O_3 and Cu nanoparticle volume fraction on the thermo-engineering fluid quantities are investigated for more significant an increasing suction ($S > 0$). A variation in φ_1 and φ_2 with the rising wall suction term

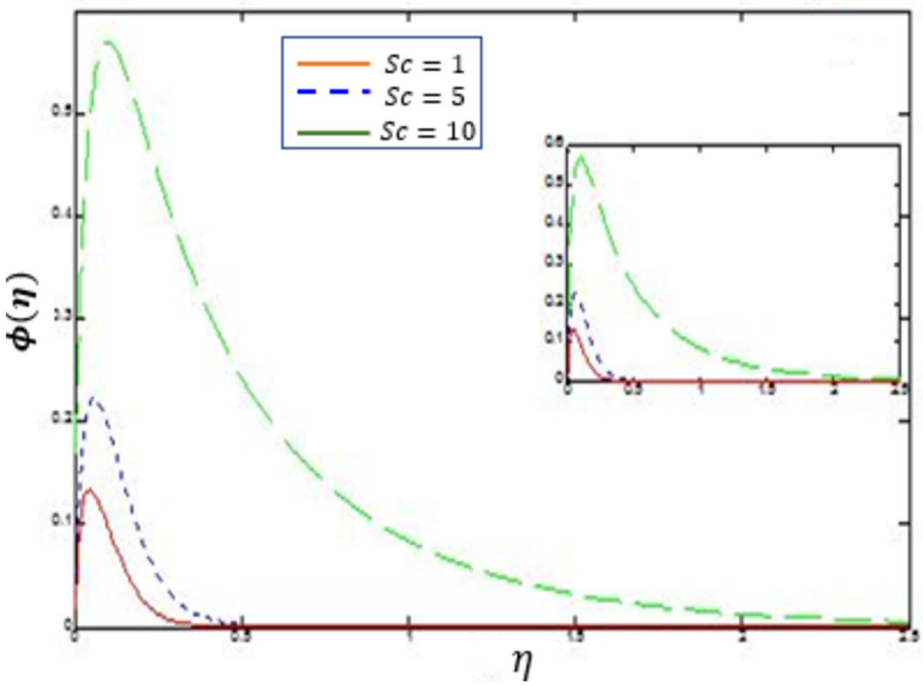

Fig. 10 Discrepancy of $\phi(\eta)$ for different values of Sc

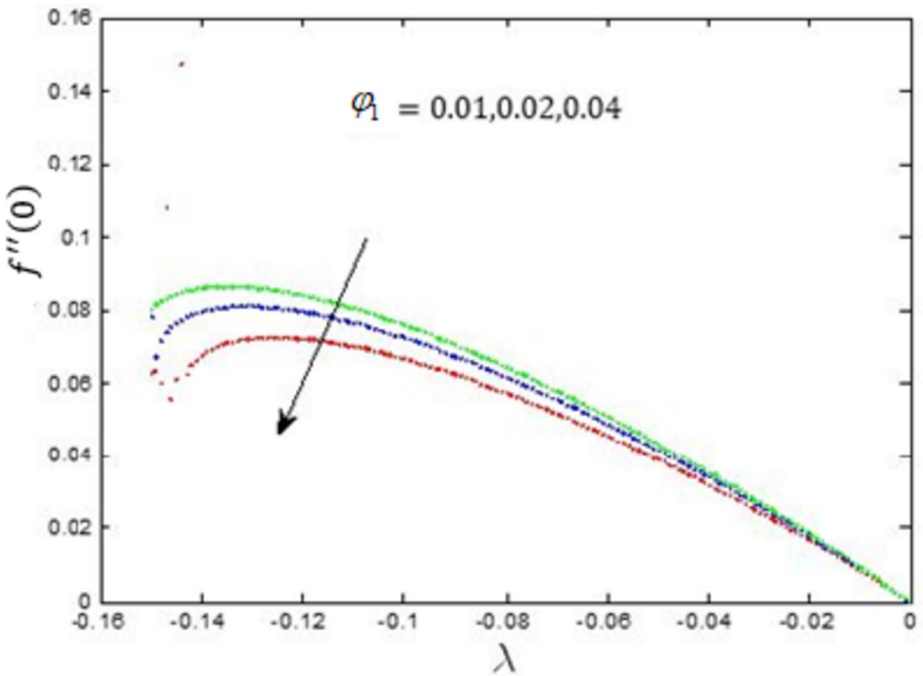

Fig. 11 Discrepancy of $f''(0)$ with λ for different values of φ_1

individually influenced the wall fluid friction, plate heat gradient, and stretchy wall concentration gradient. As displayed in Figs. 17, 18, and 19, an expanding value of Al_2O_3 volume fraction φ_1 decreased the skin friction due to shrinkage in the velocity

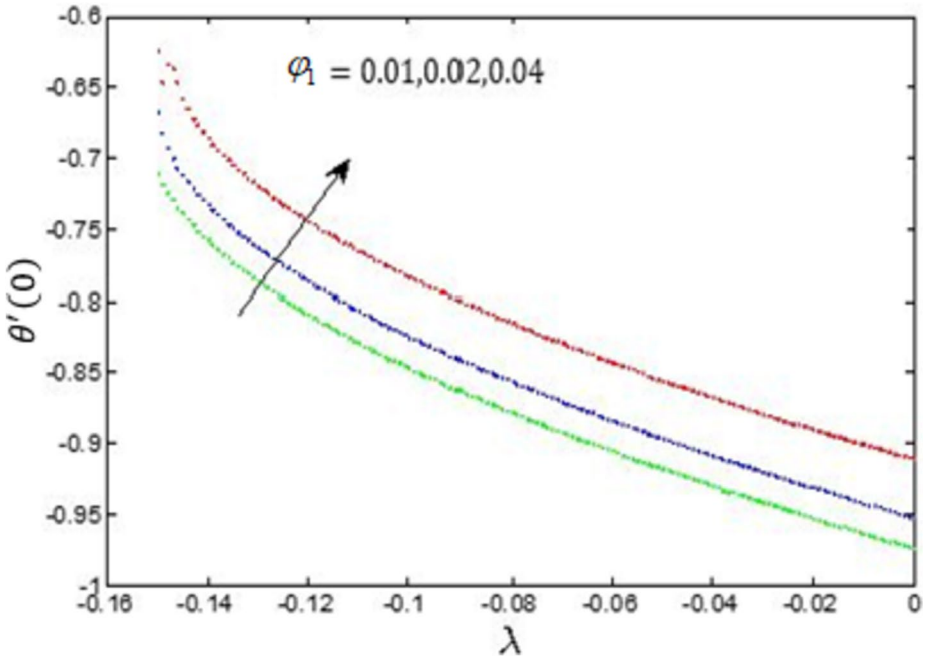

Fig. 12 Discrepancy of $\theta'(0)$ with λ for different values of φ_1

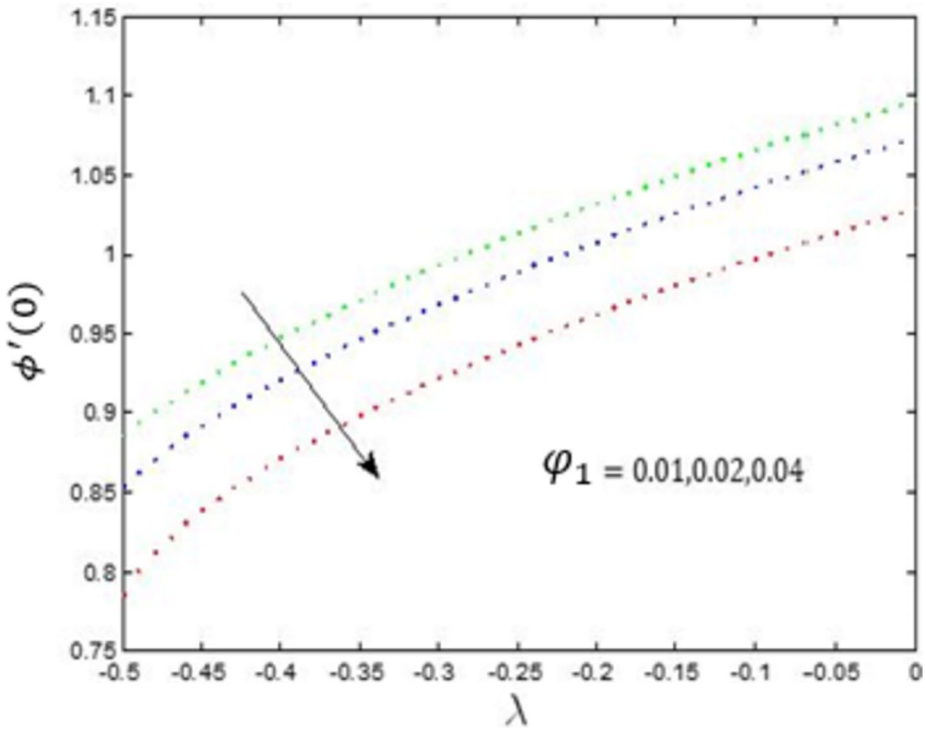

Fig. 13 Discrepancy of $\phi'(0)$ with λ for different values of φ_1

boundary viscosity, but the Nusselt number field increased due to rising nanoparticle interaction that leads to rising thermal conductivity. Meanwhile, the Sherwood number profile decreased due to a reduced mass transfer at the stretchy wall. As

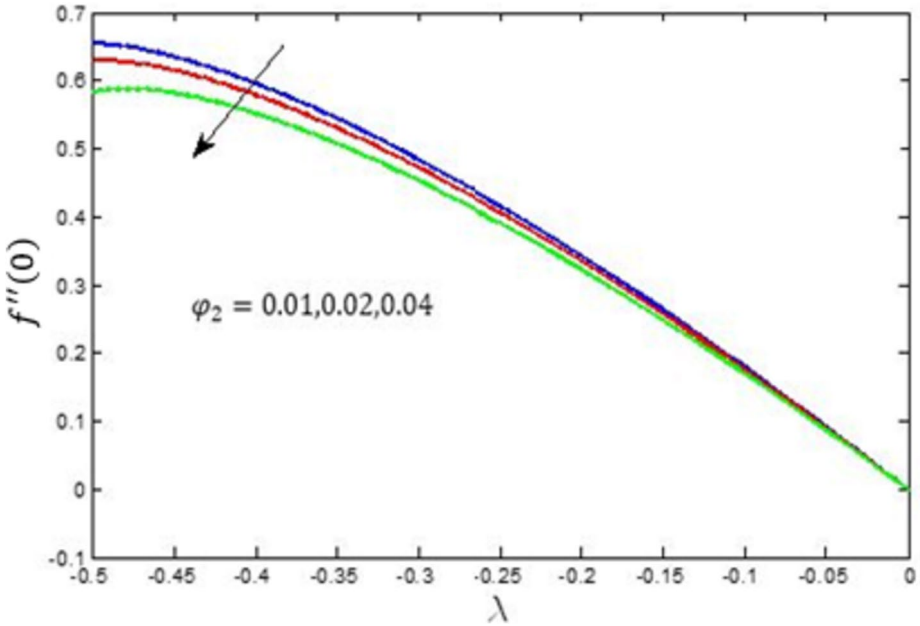

Fig. 14 Discrepancy of $f''(0)$ with λ for different values of φ_2

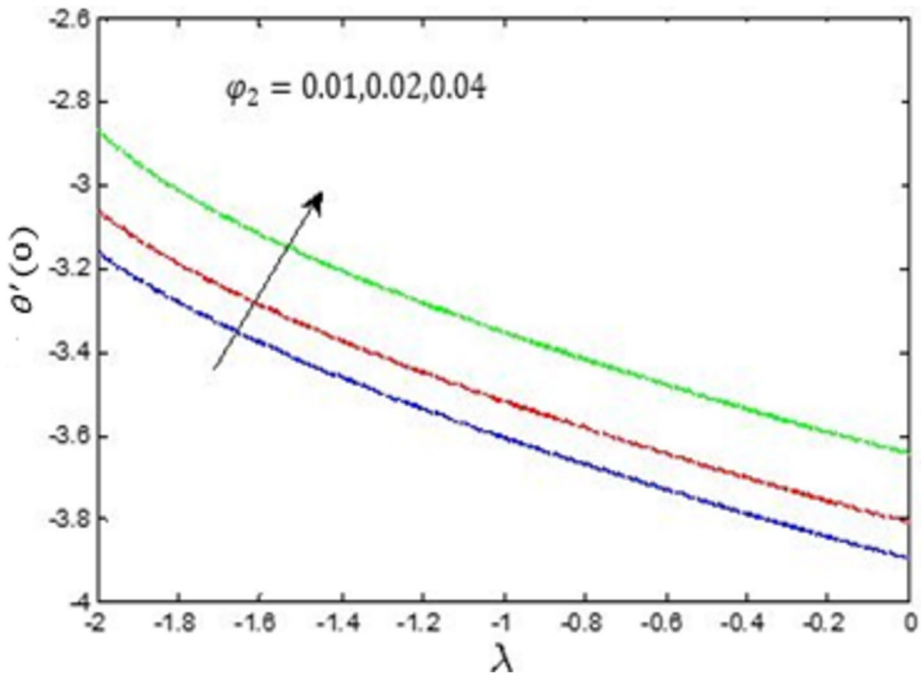

Fig. 15 Discrepancy of $\theta'(0)$ with λ for different values of φ_2

exhibited in Figs. 20, 21, and 22, increasing the Cu volume fraction φ_2 concerning rising suction term along the boundless stream correspondingly enhanced the wall friction and the thermal gradient profile as offered in Figs. 20 and 22. This resulted from the rising internal heating that propels heat transfer, thereby diminishing the

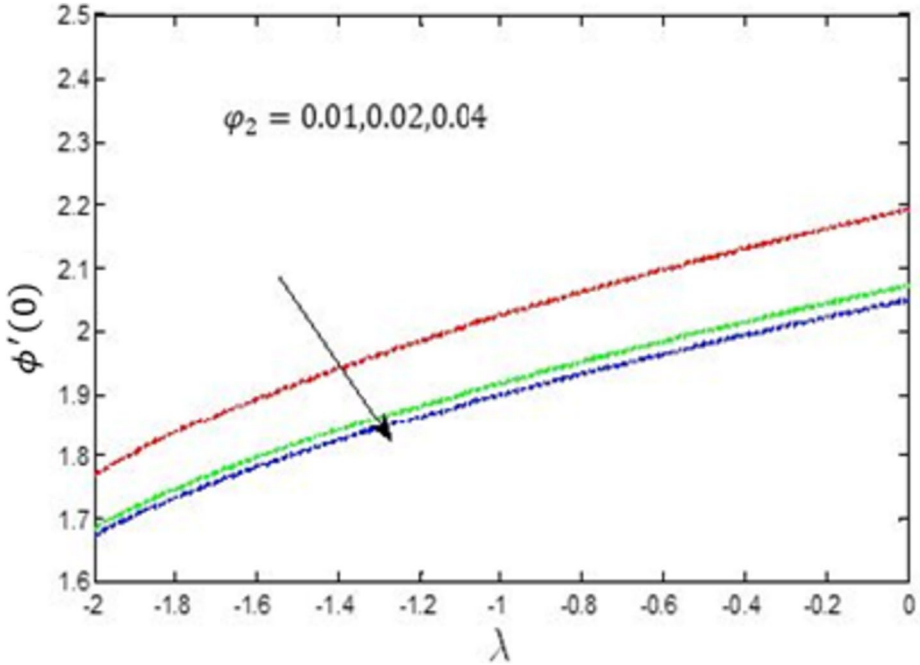

Fig. 16 Discrepancy of $\phi'(0)$ with λ for different values of φ_2

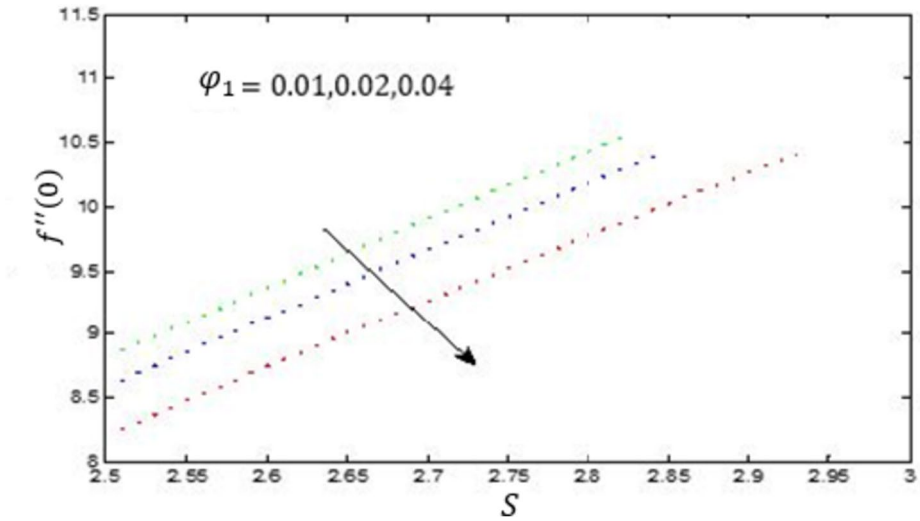

Fig. 17 Discrepancy of $f''(0)$ with S for different values of φ_1

molecular bonding. Hence, the thermophysical quantities, skin drag force, and Nusselt number profiles at the bounded flow device increased. But in Fig. 22, the chemical reaction gradient decreased along the rising suction term because of the low interaction between the Al_2O_3 and Cu nanoparticles. Therefore, the Sherwood number profile was reduced across the flow suction at the elongated sheet.

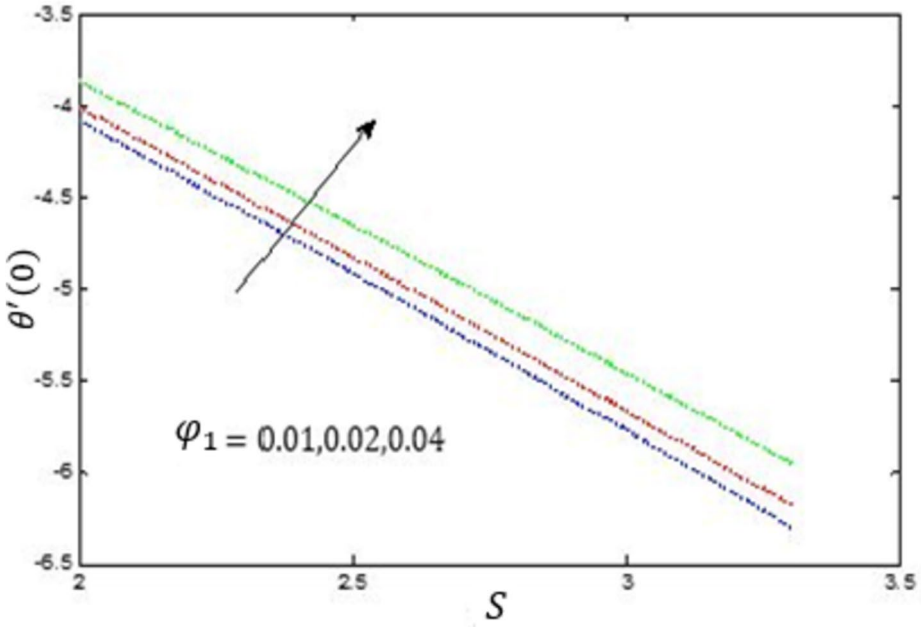

Fig. 18 Discrepancy of $\theta'(0)$ with S for different values of φ_1

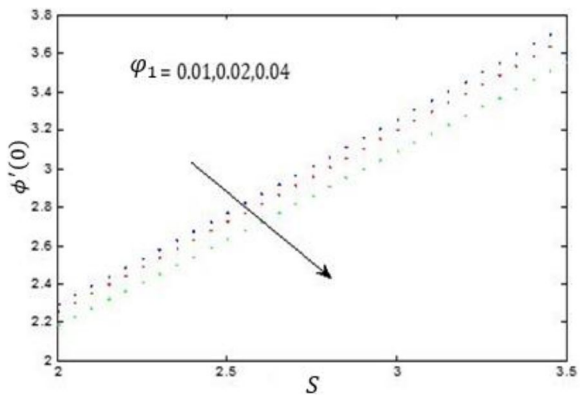

Fig. 19 Discrepancy of $\phi'(0)$ with S for different values of φ_1

Conclusions

This study uses a two-phase nanofluid model to solve the unsteady boundary layer problem of stagnation point flow of a hybrid nanofluid past a biaxial stretching/shrinking sheet. Investigation of two different nanoparticles, namely Copper and Alumina, which are diluted into water to form $Cu - Al_2O_3 -$ water hybrid nanofluid, was undertaken to make the analysis more appealing. The results for flow heat, mass transfer, and physically necessary quantities flow profiles are displayed by graphs. The main points are listed below:

- A monotonical increase in the terms λ and S with a corresponding rise in the nanoparticles Al_2O_3 and Cu volume fraction propels heat gradient rate.

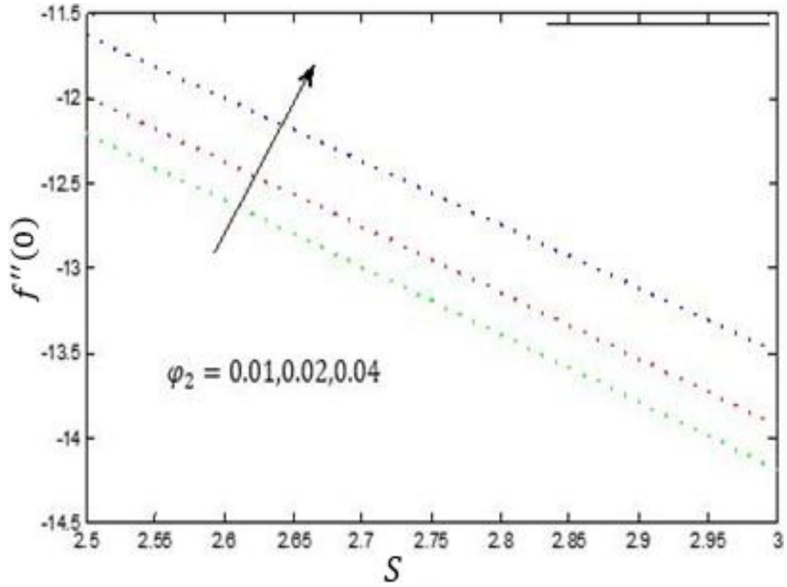

Fig. 20 Discrepancy of $f''(0)$ with S for different values of φ_2

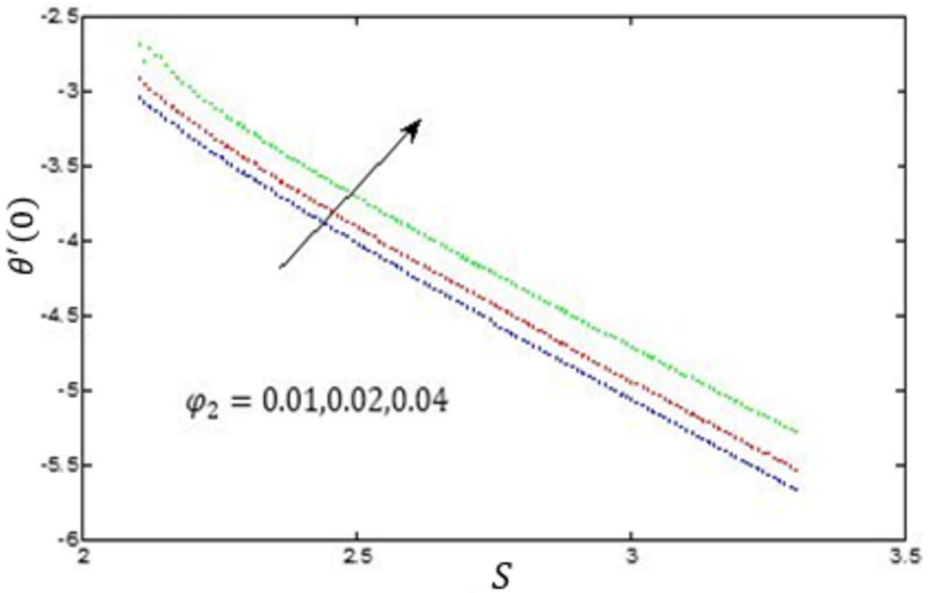

Fig. 21 Discrepancy of $\theta'(0)$ with S for different values of φ_2

- The wall friction and mass gradient reduce for a rise in the nanoparticle dispersion in water along the far streams λ and S.
- The velocity components are reduced with increasing Al_2O_3- water nanofluid volume fraction.
- Thermal conductivity of the $Al_2O_3/Cu-$ water hybridization is enhanced with expanded physical terms φ_1 and Nt.

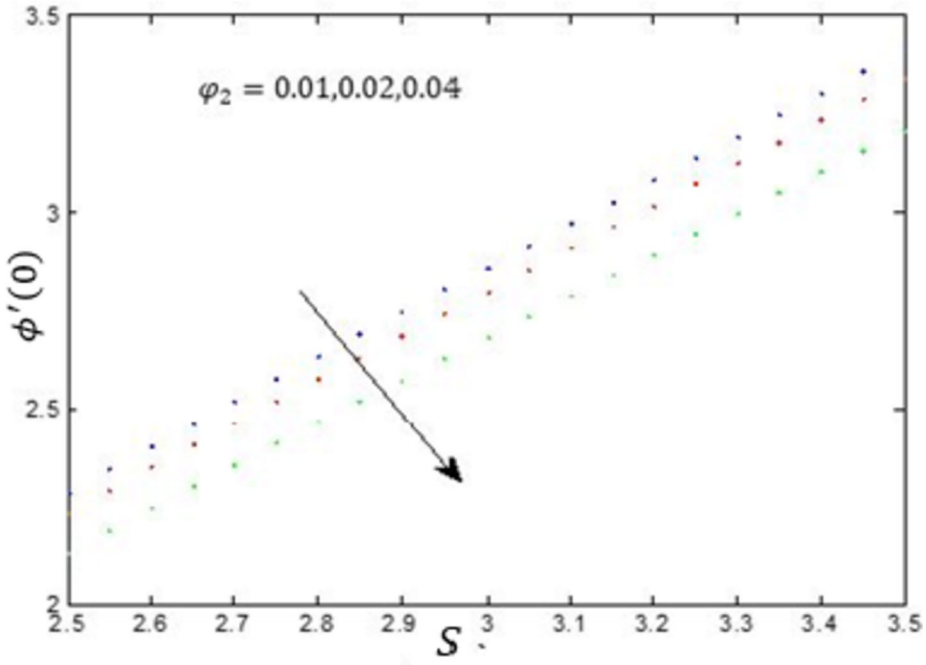

Fig. 22 Discrepancy of $\phi'(0)$ with S for different values of φ_2

- An increase in the Schmidt numbers encourages a mass transfer field due to an enhanced boundary viscosity.

The current study and the investigated flow dimension results will assist the thermal engineering and chemical production in the correct hybridization of nanofluid for improved productivity. Hence, further analysis of nanomaterials coupled with non-Newtonian fluids under various geometries is encouraged to enhance nanotechnology development.

Nomenclature

(x, y, z) Cartesian coordinates
(u, v, w) Velocity component in the x, y, and z – directions
u_e Velocity of the free stream
C_f Skin friction coefficient
C_p Specific heat at constant pressure
$(\rho C_p)_{nf}$ Heat capacitance of the nanofluid
$(\rho C_p)_f$ Heat capacitance of the fluid
$(\rho C_p)_{hnf}$ Heat capacitance of the hybrid nanofluid
ϑ_f Kinematic viscosity of the fluid
ϑ_{nf} Kinematic viscosity of the nanofluid
ϑ_{hnf} Kinematic viscosity of the hybrid nanofluid
μ_f Dynamic viscosity of the fluid
μ_{nf} Dynamic viscosity of the nanofluid

μ_{hnf} Dynamic viscosity of the hybrid nanofluid
η Dimensionless variable
$f(\eta)$ Dimensionless stream function
k Thermal conductivity of the fluid
θ*Dimensionless temperature*
λ*Stretching/shrinking parameter*
Pr Prandtl number
q_w*Surface heat flux*
Re_x Local Reynolds number
t Time
T Fluid temperature
T_w Surface temperature
T_∞ Ambient temperature
ρ_f Density of the fluid
ρ_{nf} Density of the nanofluid
ρ_{hnf} Density of the hybrid nanofluid
ψ Stream function
φ_1 Nanoparticle volume fractions for Al_2O_3 (alumina)
φ_2 Nanoparticle volume fractions for Cu (copper)

Subscripts

f Base fluid
nf Nanofluid
hnf Hybrid nanofluid
$s1$ Solid component for Al_2O_3 (alumina)
$s2$ Solid component for Cu (copper)

Acknowledgements
We appreciate the referee's comments.

Authors' contributions
We all authors made contributions in different sections and agreed to submit this paper. All authors read and approved the final manuscript.

Funding
None

Availability of data and materials
Upon request to the corresponding author.

Declarations

Competing interests
The authors declare that they have no competing interests.

Received: 18 April 2023 Accepted: 13 February 2024
Published online: 01 March 2024

References

1. Choi SUS (1995) Enhancing thermal conductivity of fluids with nanoparticles. In: Proceedings of the 1995 ASME International Mechanical Engineering Congress and Exposition, San Francisco, CA, vol 35, pp 164–177
2. Das SK, Choi SUS, Yu W, Pradeep T (2007) Nanofluids: science and technology. vol 122, no 3. Wiley Inter Science, NJ, pp 188–197

3. Minkowycz WJ, Sparrow EM, Abraham JP (eds) (2013) Nanoparticle heat transfer and fluid flow, vol 154 No.3. CRC Press, Taylor and Francis Group, New York, pp 556–564
4. Fan J, Wang L (2011) Review of heat conduction in nanofluids. ASME J Heat Transf 133(4):40801. https://doi.org/10.1115/1.4002633
5. Sarkar J, Ghosh P, Adil A (2015) A review on hybrid nanofluids: recent research, development and applications. Renew Sustain Energy Rev 43:164–177
6. Hemmat EM, Alirezaie A, Rejvani M (2017) An applicable study on the thermal conductivity of SWCNT-MgO hybrid nanofluid and price performance analysis for energy management. Appl Therm Eng 111:1202–1210
7. Sundar LS, Sharma KV, Singh MK, Sousa ACM (2017) Hybrid nanofluids preparation, thermal properties, heat transfer and friction factor – a review. Renew Sustain Energy Rev 68:185–198
8. Siddik NAC, Adamu IM, Jamil MM, Kefayati GHR, Mamat R, Najafi G (2016) Recent progress on hybrid nanofluids in heat transfer applications: a comprehensive review. Int Commun Heat Mass Transfer 78:68–79
9. Akilu S, Sharma KV, Baheta AT, Mamat R (2016) A review of thermophysical properties of water based composite nanofluids. Renew Sustain Energy Rev 66:654–678
10. Leong KY, Ku Ahmad KZ, Ong HC, Ghazali MJ, Baharum A (2017) Synthesis and thermal conductivity characteristics of hybrid nanofluids – a review. Renew Sustain Energy Rev 75:868–878
11. Devi SPA, Devi SSU (2016) Numerical investigation of hydromagnetic hybrid Cu -Al_2O_3/ water nanofluid flow over a permeable stretching sheet with suction. Int J Nonlinear Sci Num Simul 17(5):249–257
12. Devi SSU, Devi SPA (2016) Numerical investigation of three-dimensional hybrid Cu–Al_2O_3/ water nanofluid flow over a stretching sheet with effecting Lorentz force subject to Newtonian heating. Can J Phys 94(5):490–496
13. Rostami MN, Dinarvand S, Pop I (2018) Dual solutions for mixed convective stagnation-point flow of an aqueous silica–alumina hybrid nanofluid. Chin J Phys 56(5):2465–2478
14. Waini I, Ishak A, Pop I (2019) Unsteady flow and heat transfer past a stretching/shrinking sheet in a hybrid nanofluid. Int J Heat Mass Transf 136:288–297
15. Wang CY (1984) The three-dimensional flow due to a stretching flat surface. Phys Fluids 27(8):1915–1917
16. Devi CD, Takhar HS, Nath G (1986) Unsteady, three-dimensional, boundary-layer stretching surface. Int J Heat Mass Transf 29(12):1996–1999
17. Laha MK, Gupta PS, Gupta AS (1989) Heat transfer characteristics of the flow of an incompressible viscous fluid over a stretching sheet. Wärme- Und Stoffübertragung 24(3):151–153
18. Thakar HS, Nath G (1996) Unsteady three-dimensional flow due to a stretching flat surface. Mech Res Commun 23(3):325–333
19. Wang CY (2011) A fluid film sprayed on a three-dimensional stretching/shrinking sheet. Fluid Dyn Res 43(5):55501. https://doi.org/10.1088/0169-5983/43/5/055501
20. Ahmad R, Mustafa M, Hayat T, Alsaedi A (2016) Numerical study of MHD nanofluid flow and heat transfer past a bidirectional exponentially stretching sheet. J Magn Magn Mater 407:69–74
21. Wang CY (2015) Uniform flow over a bi-axial stretching surface. J Fluids Eng 137(8):84502. https://doi.org/10.1115/1.4029447
22. Buongiorno J (2006) Convective transport in nanofluids. J Heat Transfer 128(3):240–250
23. Grosan T, Pop I (2018) Flow and heat transfer over a permeable biaxial stretching/shrinking sheet in a nanofluid. Neural Comput Appl 122(3):1–8
24. Abbas N, Malik MY, Nadeem S (2020) Stagnation flow of hybrid nanoparticles with MHD and slip effects. Heat Transf 49(1):180–196
25. Nadeem S, Amin A, Abbas N (2020) On the stagnation point flow of nanomaterial with base viscoelastic micropolar fluid over a stretching surface. Alex Eng J 59(3):1751–1760
26. Abbas N, Rehman KU, Shatanawi W, Malik MY (2022) Numerical study of heat transfer in hybrid nanofluid flow over permeable nonlinear stretching curved surface with thermal slip. Int Commun Heat Mass Transf 135:106107. https://doi.org/10.1016/j.icheatmasstransfer.2022.106107
27. Li P, Duraihem FZ, Awan AU, Al-Zubaidi A, Abbas N, Ahmad D (2022) Heat transfer of hybrid nanomaterials base maxwell micropolar fluid flow over an exponentially stretching surface. Nanomaterials 12(7):1207. https://doi.org/10.3390/nano12071207
28. Abbas N, Shatanawi W (2022) Heat and mass transfer of Micropolar-Casson nanofluid over vertical variable stretching Riga sheet. Energies 15(14):4945. https://doi.org/10.3390/en15144945

Publisher's Note